Accepted Manuscript

Detection of *Aeromonas hydrophila* DNA oligonucleotide Sequence using a Biosensor Design based on Ceria Nanoparticles Decorated Reduced Graphene Oxide and Fast Fourier Transform Square Wave Voltammetry

Safiye Jafari, Farnoush Faridbod, Parviz Norouzi, Amin Shiralizadeh Dezfuli, Davood Ajloo, Fatemeh Mohammadipanah, Mohammad Reza Ganjali

PII: S0003-2670(15)00810-7

DOI: 10.1016/j.aca.2015.05.055

Reference: ACA 233974

To appear in: *Analytica Chimica Acta*

Received Date: 8 April 2015

Revised Date: 26 May 2015

Accepted Date: 30 May 2015

Please cite this article as: S. Jafari, F. Faridbod, P. Norouzi, A.S. Dezfuli, D. Ajloo, F. Mohammadipanah, M.R. Ganjali, Detection of *Aeromonas hydrophila* DNA oligonucleotide Sequence using a Biosensor Design based on Ceria Nanoparticles Decorated Reduced Graphene Oxide and Fast Fourier Transform Square Wave Voltammetry, *Analytica Chimica Acta* (2015), doi: 10.1016/j.aca.2015.05.055.

Graphical abstract

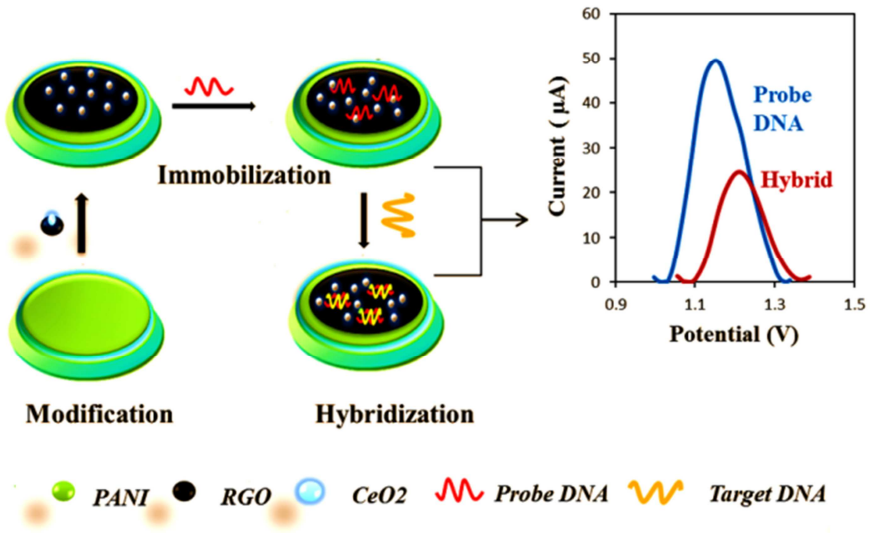

ACA-15-769R1

Detection of *Aeromonas hydrophila* DNA oligonucleotide Sequence using a Biosensor Design based on Ceria Nanoparticles Decorated Reduced Graphene Oxide and Fast Fourier Transform Square Wave Voltammetry

Safiye Jafari [a], Farnoush Faridbod [a,b,*], Parviz Norouzi [a,b], Amin Shiralizadeh Dezfuli [a], Davood Ajloo [c], Fatemeh Mohammadipanah [d], Mohammad Reza Ganjali [a,b]

[a] *Center of Excellence in Electrochemistry, University of Tehran, Tehran, Iran*

[b] *Biosensor Research Center, Endocrinology & Metabolism Molecular and Cellular Research Institute, Tehran University of Medical Sciences, Tehran, Iran*

[c] *School of Chemistry, Damghan University, Damghan, Iran*

[d] *Department of Microbial Biotechnology, School of Biology and Center of Excellence in Phylogeny of Living Organisms, College of Science, University of Tehran, 14155-6455, Tehran, Iran*

Abstract- A new strategy was introduced for ssDNA immobilization on a modified glassy carbon electrode. The electrode surface was modified using polyaniline and chemically reduced graphene oxide decorated cerium oxide nanoparticles (CeO_2NPs-RGO). A single-stranded DNA (ssDNA) probe was immobilized on the modified electrode surface. Fast Fourier transform square wave voltammetry (FFT-SWV) was applied as detection technique and $[Ru(bpy)_3]^{2+/3+}$ redox signal was used as electrochemical marker. The hybridization of ssDNA with its complementary target caused a dramatic decrease in $[Ru(bpy)_3]^{2+/3+}$ FFT-SW signal. The proposed electrochemical biosensor was able to detect *Aeromonas hydrophila* DNA oligonucleotide sequence encoding aerolysin protein. Under optimal conditions, the biosensor showed excellent selectivity toward complementary sequence in comparison with noncomplementary and two-base mismatch sequences. The dynamic linear range of this

*corresponding author: Phone: +98-21-61112788; E-mail: faridbodf@khayam.ut.ac.ir

electrochemical DNA biosensor for detecting 20-mer oligonucleotide sequence *of Aeromonas hydrophila* was from 1×10^{-15} to 1×10^{-8} mol L^{-1}. The proposed biosensor was successfully applied for the detection of DNA extracted from *Aeromonas hydrophila* in fish pond water up to 0.01 µg mL^{-1} with RSD of 5%. Besides, molecular docking was applied to consider the $[Ru(bpy)_3]^{2+/3+}$ interaction with ssDNA before and after hybridization.

Keywords: Biosensor, *Aeromonas hydrophila*, Graphene oxide, Cerium oxide, Fast Fourier transforms, Square wave voltammetry

1. Introduction

Recently, the research area of DNA hybridization biosensors has found an important place in the diagnosis of genetic and infectious diseases, genotyping, bacterial and viral analysis and food safety monitoring [1]. Generally, a DNA biosensor comprises a single-stranded oligonucleotides (ssDNA) immobilized on a transducer surface, which can then recognize its complementary sequence via hybridization event [2]. Many selective and sensitive detection techniques, based on different signal transduction, including optical, piezoelectric and electrochemical read outs have been developed [3]. Among them, electrochemical methods attract more attentions for use in point-of-care clinical diagnostic devices due to their fast, simple, sensitive, low cost detection and ease of miniaturization [4,5].

The configuration of the recognition layer is a critical step in designing a DNA biosensor [6,7]. One of the important approaches for immobilization of DNA sequence on the electrode surface (especially gold or gold nanoparticles modified electrodes) is using thiolated ssDNA. However, this process is expensive and labor consuming. Biocompatible nanomaterial is largely used to modify the electrode surfaces in order to obtain high hybridization efficiency and decrease non-specific adsorption of ssDNA [8,9].

The proposed nanocomposite in this study can be a new and easy approach for immobilization of ssDNA on the electrode surface without using any functionalization or mediators.

Polyaniline (PANI) is a highly conductive polymer with good environmental stability and biocompatibility. Its application in DNA biosensor design is becoming increasingly popular since it can provide a large surface area and excellent electrical conductivity, which can facilitate the signal transduction. Moreover PANI can interact with graphene sheets through π-π stacking [10,11]. Graphene is single-atom sheets of sp^2 Carbons which has an extremely large surface area, excellent thermal and electrical conductivity [12,13]. It has been used for immobilizing of DNA probe via non-covalent interaction (π-π stacking) between its conjugated interface and DNA bases [14,15]. Further modification strategies were using graphene-metal nano-composites [16,17]. Among metal nanoparticles CeO_2 (called Ceria) is particularly attractive because of its high catalytic activity and biocompatibility [18,19]. It has been used for immobilizing of DNA probe via non-covalent interaction (π-π stacking) between its conjugated interface and DNA bases [20].

Square wave voltammetry (SWV) is a sensitive electrochemical technique that has been extensively used as detection technique in designing biosensors [21-23]. In SWV measurements, the detection limits can be drastically improved. SWV measures the current response while rapid alternating potentials are applied during a staircase scan. Moreover, fast Fourier transform (FFT) in combination with SWV technique has shown excellent sensitivity [24,25]. The approach is designed to separate the voltammetric signal and background signal in frequency domain using

discrete fast Fourier transformation (FFT) method. Therefore, some of the environmental noises was digitally filtrated that could improve the detection limit [24-26].

The ssDNA used in this work is a 20-mer oligonucleotides sequence that has been previously verified and reported to have high selectivity and specificity to *A. hydrophila* aerolysin gene [27]. *A. hydrophila* is a highly epidemic pathogen, mostly distributed in aquatic environments and food. This opportunistic pathogen is a gram-negative, rod-shaped bacterium that is classified as an emerging pathogen [28]. The pathogenicity of *A. hydrophila* was believed to be mediated mainly by an extracellular protein, aerolysin, which its encoding gene is used for identification of this bacterium by polymerase chain reaction (PCR) [29,30]. The microgravimetric (QCM, quartz crystal microbalance) biosensor coupled with PCR was used for detection of aerolysin gene fragments [31]. Although these methods provide efficient detection of *A. hydrophila*, they were time consuming, complicated and has not too low detection limit. Recently, electrochemical DNA biosensors have been also used to identify aerolysin gene (with various sequences). In all of them labeled ssDNA were used which has a difficult and expensive biochemical preparation [27,32,33].In this study, we used a new methodology for immobilization of ssDNA sequence on glassy carbon electrode. Reduced graphene oxide decorated cerium oxide nanocomposite/Polyaniline/glassy carbon electrode [CeO_2NPs-RGO/PANI/GCE] was fabricated as a platform for immobilization of ssDNA sequence. By employing this method, the interaction of captured ssDNA on the electrode surface got much stronger. The hybridization process was monitored by the FFT-SW redox current signal of $[Ru(bpy)_3]^{2+/3+}$. Under optimal experimental condition, the proposed DNA biosensor showed high sensitivity and selectivity toward the detection of a 20-mer oligonucleotides

sequence related to *A. Hydrophila.* Besides the experimental studies, molecular docking was applied to explain the interaction of $[Ru(bpy)_3]^{2+/3+}$ with ssDNA before and after hybridization.

2. Materials and methods

2.1. Apparatus

Voltammetric measurements (CV and FFT-SW) were performed using a homemade potentiostat connected with a three-electrode system consists of a glassy carbon electrode (GCE) and modified electrode, an Ag/AgCl reference electrode and a platinum wire as an auxiliary electrode. The potentiostat was connected to a PC equipped via a data acquisition board (PCL-818H, Advantech Co.), used to control the potential of potentiostat and acquire current readings. Software was developed using Delphi 6.0 to apply repeatedly a waveform to the working electrode and synchronously acquire, analyze, and store the current data. The controlling program was accompanying dynamic link libraries allowed waveform generation and current sampling to be synchronized, which was essential in interpreting SWV current response [24-26]. Electrochemical impedance measurements were carried out on AUTOLAB PGSTAT 30. Phase compositions of the samples were characterized by X-ray diffraction (XRD) on a Philips PW-1730 X-ray diffractometer using Cu Kα radiation (λ=1.5405Å). Scanning electron microscopy (SEM) measurement was carried out on a Zeiss SIGMA VP scanning electron microscope.The pH values of all solutions were measured by a model SAT-2100 pH meter (Sabalan Azmai Tehran Co., Ltd, Iran).

2.2. Materials & Reagents

All the chemical reagents were of analytical grade and all solution were prepared using deionized water. All oligonucleotides were purchased from Generay Biotech CO., Ltd. (Shanghai, China). The DNA stock solutions were prepared with TE buffer (10 mM Tris-HCl, 1mM, EDTA, pH 8.00) and kept frozen. More dilute solutions were prepared with 10 mmol L^{-1} Tris-HCl buffer containing 10 mmol L^{-1} NaCl pH 7.40.

ssDNA probe: 5′- GTGGTGGGCTGGGCGATCAA-3′

Target DNA (fragments of *A. hydrophila* aerolysin previously reported) [27]:

5′-TTGATCGCCCAGCCCACCAC -3′

Mismatch (MM*):* 5′- TTGATCGC**T**CAGC**A**CACCAC -3′

Non-complementary DNA:

5′- GCATGACGTTATTTATGAGAT-3′

The *A. hydrophila* strain was provided by the University of Tehran Microorganisms Collection (UTMC). Polyaniline (PANI) solution was synthesized sonochemically [34,35]. In brief, the purified aniline (1.14 mL) was dissolved in 50 mL of 1 M HCl aqueous solution. While maintaining vigorous stirring at room temperature, 50 mL of 0.25 mol L^{-1} ammonium peroxydisulfate solution was quickly poured into the aniline solution followed by a 2 h mixing in an ultrasonic bath in 4^{o} C. The green emeraldine salt was washed with distilled water and HCl until the filtrate was colorless. Then, the precipitate was dried in vacuum oven at 60^{o} C for 24 h.

2.3. Preparation of CeO_2NPs -RGO nanocomposite

The CeO_2NPs-RGO nanocomposite was prepared by a facile sonochemical method [36]. The preparation procedure used in the present study was briefly as follows. Firstly, an amount of $Ce(NO_3)_3.6H_2O$ (1 mmol) was dissolved in deionized water (30 mL). Then, during the ultrasound irradiation (in an ultrasonic bath), a 32% NH_4OH aqueous solution (2 mL) was added drop-wise to the above solution. This process was completed within 66 min. Secondly, 60 mL of GO suspension (0.5 mg mL^{-1}), was added to the mixture suspension and was heated to 90 ˚C, then 3 mL N_2H_4 was added and the mixture suspension was refluxed for 1 h. The resulting precipitate was washed several times with ethanol and distilled water before drying at 60 ˚C for 24 h. Finally, the obtained products were designated as CeO_2NPs-RGO.

2.4. Fabrication of CeO_2NPs-RGO nanocomposite/PANI /GCE

The GCE was polished with 0.3 µm and 0.05 µm alumina powders, respectively. Then, cleaned ultrasonically in 0.01 M NaOH solution and dried with blowing N_2 gas. 7 µL of PANI suspension (0.04 mg mL^{-1}) was dropped on the electrode surface and dried using an IR lamp. Then, 7 µL of (CeO_2-RGO) nanocomposite suspension (0.5 mg mL^{-1} and 1:2, the mass ratio of CeO_2: G) was dropped on PANI/GCE surface and dried under the IR lamp.

2.5. Probe DNA immobilization and hybridization

7 µL of 7.5 µmol L^{-1} ssDNA solution was dropped on the modified electrode surface and kept for 30 min at room temperature. Then, the ssDNA/ CeO_2NPs-RGO/ PANI/ GCE were rinsed with buffer for 5 seconds to prevent nonspecific adsorption of ssDNA. The

DNA hybridization reaction was performed by dropping 7 µL of appropriate concentration of target DNA solution on ssDNA/ CeO_2NPs-RGO/PANI/GCE interface and the reaction was kept for about 1 h. Then, the electrode was rinsed by buffer for 10 seconds to remove the unhybridized target DNA.

2.6. Electrochemical measurements

The electrochemical measurements of the modified electrodes were done by FFT square wave voltammetry (FFT-SW), cyclic voltammetry (CV) and impedance spectroscopy (EIS). FFT-SWV data collection involves sampling of the measured parameter, potential or current, at predetermined intervals for a required number of samples. The number of samples taken, i.e. the length of the time record, determines the lowest frequency that may be reliably measured in the collected data and is largely determined by the storage capacity and speed of the computer used. The measurement waveform contains multiple SW pulse cycles with an amplitude of E_{sw} and frequency of *f*o, superimposed on a staircase potential function, and changed by a small potential step of ΔE. It is required that the number of sampled currents at each pulse cycle be represented by 2*n* (where *n* is an integer and greater than 1). The EIS was performed at AC voltage amplitude of 5 mV, the applied potential of 0.3 V *vs.* Ag/AgCl, and the frequency range from 100 kHz to 0.1 Hz. The electrode was immersed into the Tris-HCl buffer (10 m mol L^{-1} Tris-HCl, 10 mmol L^{-1} NaCl, pH 7.4) containing 20 µmol L^{-1} $[Ru(bpy)_3]^{2+/3+}$ stirring at 250 rpm for 5 min. Then, it was rinsed with buffer for 5 seconds. The FFT-SW signal of accumulated $[Ru (bpy)_3]^{2+/3+}$ was measured in Tris-HCl buffer pH 7.40. The CV and EIS

measurements were carried out in 10 m mol L^{-1} $[Fe(CN)_6]^{3-/4-}$ solution containing 0.1 mol L^{-1} KCl.

2.7. Molecular Docking

AutoDock 4.2.0 software was used for the ligand docking to receptor. The structure of $[Ru(bpy)_3]^{2+/3+}$ complex was optimized by Gaussian 09 and imported into ADT. Polar hydrogens were added, Gasteiger charges were computed; and the rigid root and the rotatable bonds were defined by the AutoTors tool of ADT [37]. The grid module was employed to create grid maps with 52×110×80 points and a grid-point spacing of 0.375 nm. For each complex, 200 independent docking runs were conducted. The settings of the parameters were as follows: population size of 50, a maximum number of 25 million energy evaluations, a maximum number of 27,000 generations, a crossover rate of 0.8, and a mutation rate of 0.02 were set up. The docking results were clustered according to a root-mean square deviation (RMSD) criterion of 0.5 and evaluated depending on the docking free energy.

2.8. Real sample analysis

For real sample analysis, the genomic DNA was extracted from bacteria using phenol-chloroform protocol [38]. Fish pond water sample were filtrated with 0.45 µm filter. The filtrated was then used to prepare different concentration of the *A. hydrophila* genome (from 10 to 0.01 µg mL^{-1}). Before the hybridization process, DNA was denatured at 95 ˚C for 1 min into single strands.

3. RESULT AND DISCUSSION

3.1. Structural and morphological characterization

The crystal phase of the prepared CeO_2NPs-RGO nanocomposite was examined by x-ray diffraction (XRD). As shown in Fig. 1, the diffraction peaks at 28.58, 33.17, 47.50, 56.41, 59.14, 69.49, 76.80, 79.21, and 88.38, which correspond to (111), (200), (220), (311), (322), (400), (331), (420), and (422) planes, respectively. This pattern matches with a typical cubic fluorite-type structure of CeO_2 (JCPDS no. 34-0394), indicating that CeO_2 nanoparticles were successfully anchored on the RGO.

<Fig. 1. >

As observed in FE-SEM image (Fig. 2), a large number of CeO_2 nanoparticles have been attached to the RGO surface with a good dispersion, indicating a good combination between nanoparticles and RGO. Fig. 2 shows the CeO_2 nanoparticles before and after combining with RGO. Through this combination, the agglomeration of CeO_2 nanoparticles can be prevented effectively. It is also suggested that the CeO_2 nanoparticles on the RGO's surfaces can act as spacers and thus prevent the RGOs to restack [36]. Thus, it can increase the stability of the single- or few-layers exfoliated RGO and introduces a much more surface area in the nano-composite [39,40].

<Fig. 2. >

3.2. Electrochemical characterization of biosensor

The redox peaks current of $[Fe(CN)_6]^{3-/4-}$ couple is extensively used as an electrochemical marker to determine the characteristic of electroactive materials [41]. Fig. 3A displays the CVs of differently modified electrodes: bare GCE (a), CeO_2NPs-RGO/PANI/GCE (b) and

ssDNA/CeO_2NPs -RGO /PANI/GCE before (c) and after hybridization with target DNA (d) in 10 mmol L^{-1} $[Fe(CN)_6]^{3-/4-}$ containing 0.1 mol L^{-1} KCl at 100 mV/s. A couple of redox peaks can be observed in all CV plots. As expected, the current responses of CeO_2NPs-RGO/PANI/GCE increased notably compared to those of bare GCE but with slight change in ΔE_p. It indicates that the electron transfer rate at the electrode surface was accelerated because of the large surface area and excellent electrical conductivity of the nanocomposite film. After immobilization of the ssDNA probe on the modified electrode, the peaks current decreased and ΔE_p increased notably, this can be attributed to the electrostatic repulsion between the negatively charged ssDNA and $[Fe(CN)_6]^{3-/4-}$ anions. After hybridization, the negative charge on the electrode surface increased. As a result, the current of the peaks further decreased and ΔE_p increased [42]. The electroactive surface area of the electrodes was calculated according to Randles–Sevcik equation;

$$i_{pa} = 2.69\times10^5 A D^{1/2} n^{3/2} \nu^{1/2} C, \qquad (1)$$

Where i_{pa} is the anodic peak current, n the electron-transfer number, A the surface area of the electrode, D the diffusion coefficient, C the concentration of $[Fe(CN)_6]^{3-/4-}$ and ν the scan rate [43]. For the solution of $[Fe(CN)_6]^{3-/4-}$, n=1, D= 6.70×10^{-6} cm^2/s, then from the slope of the i_{pa}-$\nu^{1/2}$ plot, the surface area value of bare GCE, CeO_2NPs-RGO/PANI/GCE, ssDNA/CeO_2NPs-RGO/PANI/GCE before and after hybridization with target DNA was being calculated to be 0.027, 0.044, 0.023, 0.018, respectively. It is clear that the CeO_2NPs-RGO /PANI/GCE surface area is higher than that of the corresponding bare electrode, indicating the effect of (CeO_2-RGO) nanocomposite and PANI on enhancing the electroactive surface area of modified electrode.

The EIS is a practical technique to study the electrochemical characteristic of the modified electrode surfaces. As a rule, the semicircle part of the Nyquist diagram correlates with the electron-transfer limiting process. The charge-transfer resistance (R_{ct}) value at the modified electrode can be directly measured as the semicircle diameter [44]. As shown in Fig. 3B the R_{ct} value of CeO_2NPs-RGO/PANI/GCE (115 Ω) declined dramatically in comparison with bare GCE (275 Ω) which indicate that the (CeO_2-RGO)/PANI film speeded up the interfacial electron transfer process. After immobilization of ssDNA probe, the interfacial R_{ct} increased greatly to 500 Ω, due to its negatively charged phosphate backbone which is repulsive to anionic electrochemical probes like $[Fe(CN)_6]^{3/4-}$. After hybridization, the R_{ct} value further increased to 650 Ω which was attributed to more negative charges at the electrode surface that would make the interfacial electron transfer even more difficult [33]. The results were consistent with those obtained from CV measurements.

<Fig. 3. >

3.3. Optimization

Since the amount of immobilized DNA probe substantially affects the sensitivity of the DNA biosensor, the effect of DNA probe concentration on the response signal was investigated. As Fig. 4A illustrated, the response signal gradually increases with increasing the DNA probe concentration to 7.5 µmol L^{-1} and then dramatically decreases. Therefore, we used ssDNA probe at a concentration of 7.5 µmol L^{-1} in this study.

Another important parameter which can affect a DNA biosensor sensitivity is hybridization time. As shown in Fig. 4B, the response signal of biosensor increased as the hybridization time increased up to 60 min. After 60 min, the response signal remained

steady, indicating that the hybridization reaction was almost completed. Therefore, we used 60 min as the optimum hybridization time.

<Fig. 4. >

3.4. Analytical performance of the biosensor

In this study, the difference in FFT-SW signal of the accumulated $[Ru(bpy)_3]^{2+/3+}$ at the modified electrode surface with single-stranded DNA probes, before and after the hybridization process was considered as the response signal of the biosensor (ΔI). The signal of the biosensor after hybridization with target DNA decreased, significantly. In the absence of the target sequence, $Ru(bpy)_3^{2+}$ is oxidized to $Ru(bpy)_3^{3+}$ on the electrode surface. The guanine bases of ssDNA then reduced $Ru(bpy)_3^{3+}$ to regenerate $Ru(bpy)_3^{2+}$ forming a catalytic cycle as shown below [45].

$$Ru(bpy)_3^{2+} \rightarrow Ru(bpy)_3^{3+} + e^- \quad (1)$$

$$Ru(bpy)_3^{3+} + DNA \rightarrow DNA_{ox} + Ru(bpy)_3^{2+} \quad (2)$$

After DNA hybridization occurres, as the EIS data shown in Fig. 3B, the resistance of the electrode surface increases which is the major reason of the current decrease. In addition, due to participation of the guanine bases of ssDNA in the double helix structure, they are less available to $[Ru(bpy)_3]^{2+/3+}$. Therefore, the catalytic reaction is prohibited and the peak current decreases [45,46]. Moreover, because of the increasing the negative charge of double strand DNA, a more stronger interaction of $[Ru(bpy)_3]^{2+/3+}$ with double helix occures. Molecular docking studies also showes the stucking of $[Ru(bpy)_3]^{2+/3+}$ in major grooves of DNA double helix. Thus, the decrease in the current signal and the potential

shift to more positive values after hybridization might be attributed to the more difficult oxidation of $[Ru(bpy)_3]^{2+/3+}$ at the electrode surface with higher resistance.

3.4.1. Calibration curve

The analytical performance of the DNA biosensor was investigated using the DNA probe to hybridize with different concentration of target DNA. From Fig. 5A it is clear that the peak current decreases as the concentration of target DNA increases. As shown in Fig. 5B, inset, the response signal (ΔI) showed a good linear correlation with the logarithm of the concentration of the target DNA in the range of 1×10^{-15} to 1×10^{-8} mol L^{-1} [47]. The regression equation was ΔI=4.0001logC +69.958 [ΔI (μA), C (M)] and R^2=0.990. The detection limit was obtained 1×10^{-16} mol L^{-1} using 3σ, where σ is the standard deviation of the blank solution, n=5 and RSD 4%.

<Fig. 5. >

3.4.2. Selectivity of the DNA biosensor

The selectivity of the proposed biosensor was investigated by comparing the response signal of the biosensor before and after hybridization with noncomplementary, two-base mismatch and target sequences. As shown in Fig. 6, the highest signal was observed at ssDNA/CeO_2NPs-RGO/PANI/GCE (a, 49.49 μA) which indicated the most amount of free ssDNA on the electrode surface. The slight decrease in peak current of $[Ru(bpy)_3]^{2+/3+}$ on ssDNA/CeO_2NPs-RGO/PANI/GCE hybridized with

noncomplementary DNA (b, 46.93 µA) shows that hybridization did not occur. The lower signal for two-base mismatch DNA (c, 36.1 µA) indicates that the hybridization had not been completely accomplished. It is clear that the lowest signal belongs to target DNA (d, 24.46 µA) with respect to complete hybridization. The RSD of five replicate measurements was 5%.

<Fig. 6>

3.4.3. Stability and reproducibility of the DNA biosensor

The ssDNA/CeO_2NPs-RGO)/PANI/GCE was immersed in Tris-HCl buffer pH 7.4 for 60 min. Then, the FFT-SW signal of $[Ru(bpy)_3]^{2+/3+}$ was recorded. The response signal 3% decreased. Moreover, the ssDNA/CeO_2NPs-RGO/PANI/GCE was stored at 4 ^{0}C during 24 h for 1 week. The decrease in the biosensor response signal was 3.65 and 10%, respectively, indicating the good stability of the biosensor. The reproducibility of the biosensor was also investigated under optimum conditions. Ten ssDNA/CeO_2NPs-RGO/PANI/GC electrodes were fabricated to detect 1×10^{-12} mol L^{-1} of target DNA. The average value of ten measurments was 20.45± 1.66 indicating the good reproducibility of the biosensor.

3.5. Molecular Docking

The 200 docking energies in 9 and 17 cluster ranks for single and double strands were listed in Table 1. The most negative ranks are in the first row of the table so that they

have sorted from the most negative to less negative values. In comparison, between docking energies for single and double strands, it was shown that latter case has more negative energy and so higher tendency for interaction with complex. It may be due to the higher number of atoms that engage in complex binding.

Fig. 7 shows the structure of single and double strands as well as of 200 docking sites in 9 and 17 cluster ranks. $[Ru(bpy)_3]^{2+/3+}$ locate in the major groove because it is relatively large to locate in the minor groove or intercalated between base pairs. Part c and f represent the electrostatic surface of DNA and complex. White and red colors are representative of neutral and negative charges.

<Table 1>

<Fig. 7>

Figs. 8a and 8b show the closest residues to the complex in which number of residues are higher in double strand relative to the single strand case. This figure also confirms the result of Table 1 that double strand has more negative values of docking energy and a higher tendency to bind complex. Figs. 8c and 8d depict the electrostatic surface of complex and docking site residues. The surface of the complex was periphered by pyridine groups (white color). In this case, the hydrophobic interactions have a deterministic role in ligand binding.

As molecular docking study shows, the $[Ru(bpy)_3]^{2+/3+}$ complex binds to double stranded DNA and stuck in major grooves. It can be the reason why $[Ru(bpy)_3]^{2+/3+}$ oxidation reaction occurs in more positive potentials.

<Fig. 8>

3.6. Detection of *A. hydrophila* in fish pond water

In order to test the biosensor applicability for the real sample analyses, the biosensor was confronted to detect non-amplified extracted DNA isolated from *A. hydrophila* strain UTMC 2268. The samples were prepared as described in section 2.8. As shown in Fig. 9, the biosensor can detect the non-amplified extracted DNA up to 0.01 µg mL^{-1} in fish pond water, while the lowest detectable concentration of DNA by conventional electrophoresis method was about 60 µg mL^{-1}. From Table 2, it would observe that the present biosensor showed higher sensitivity and lower detection limit in real sample analysis compared to previous works, which could be attributed to enhancement of S/N ratio using FFT-SW as well as strong interaction of nanocomposite film and DNA sequences.

<Table 2>

<Fig. 9>

4. Conclusion

The DNA biosensor presented in this work, offers a simple, inexpensive, fast and reliable technique for immobilization of ssDNA on glassy carbon electrode for detection of *A. hydrophila*. A very sensitive and selective immobilization platform was developed using CeO_2NPs-RGO nanocomposite. $[Ru(bpy)_3]^{2+/3+}$ electrochemical probe was used for hybridization detection. The results showed a positive peak shift of $[Ru(bpy)_3]^{2+/3+}$ after the hybridization reaction that attributed to more difficult oxidation of $[Ru(bpy)_3]^{2+/3+}$ on the electrode surface. It was found that the biosensor discriminated noncomplementary

and two-base mismatch DNA sequences as well. Also, molecular docking showed the strong interaction of $[Ru(bpy)_3]^{2+/3+}$ with hybrid DNA. Under optimum conditions, the proposed biosensor detected 20-mer oligonucleotides related to *A. hydrophila* in linear range of 1×10^{-15} to 1×10^{-8} mol L^{-1} with detection limit of 1×10^{-16} mol L^{-1}. This method was able to detect *A. hydrophila* extracted DNA in real fish pond water sample up to 0.01 μgmL^{-1}. The proposed biosensor can be applied further for clinical diagnosis, food safety and environmental monitoring.

Acknowledgements

We gratefully acknowledge the University of Tehran for financial support of this work (GN: 6102027).

References

[1] E.L. Wong, Recent trends in DNA biosensing technologies, Biophys. Rev. Lett. 2 (2007) 167-189.

[2] P. De-los-Santos-Alvarez, M.J. Lobo-Castanon, A.J. Miranda-Ordieres, P. Tunon-Blanco, Electrochemistry of Nucleic Acids at Solid Electrodes and Its Applications, Electroanalysis 16 (2004) 1193-1204.

[3] T.G. Drummond, M.G. Hill, J.K. Barton, Electrochemical DNA sensors, Nat. Biotechnol. 21 (2003) 1192-1199.

[4] K.J. Odenthal, J.J. Gooding, An introduction to electrochemical DNA biosensors, Analyst 132 (2007) 603-610.

[5] A. Liu, K. Wang, S. Weng, Y. Lei, L. Lin, W. Chen, X. Lin, Development of electrochemical DNA biosensors, Trends Anal. Chem. 37 (2012) 101-111.

[6] J. Wang, Electrochemical nucleic acid biosensors, Anal. Chim. Acta 469 (2002) 63-71.

[7] E.L. Wong, E. Chow, J.J. Gooding, Electrochemical DNA Biosensors Exploiting Changes in the Charge Transfer Properties of DNA, Langmuir 21 (2005) 6957-6965.

[8] A. Erdem, Nanomaterial-based electrochemical DNA sensing strategies, Talanta 74 (2007) 318-325.

[9] K. Xu, J. Huang, Z. Ye, Y. Ying, Y. Li, Recent Development of Nano-Materials Used in DNA Biosensors, Sensors 9 (2009) 5534-5557.

[10] F. Hu, S. Chen, C. Wang, R. Yuan, Y. Xiang, C. Wang, Multi-wall carbon nanotube-polyaniline biosensor based on lectin–carbohydrate affinity for ultrasensitive detection of Con A, Biosens. Bioelectron. 34 (2012) 202-207.

[11] M. Du, T. Yang, X. Li, K. Jiao, Fabrication of DNA/graphene/polyaniline nanocomplex for label-free voltammetric detection of DNA hybridization, Talanta 88 (2012) 439-444.

[12] T. Kuila, S. Bose, P. Khanra, A.K. Mishra, N.H. Kim, J.H. Lee, Recent advances in graphene-based biosensors, Biosens. Bioelectron. 26 (2011) 4637-4648.

[13] M. Pumera, Graphene-based nanomaterials and their electrochemistry, Chem. Soc. Rev. 39 (2010) 4146-4157.

[14] T. Yang, Q. Li, X. Li, X. Wang, M. Du, K. Jiao, Freely switchable impedimetric detection of target gene sequence based on synergistic effect of ERGNO/PANInanocomposites, Biosens. Bioelectron. 42 (2013) 415-418.

[15] Z. Xu, B.R. Meher, D. Eustache, Y.J. Wang, Insight into the interaction between DNA bases and defective graphenes: covalent or non-covalent, Mol. Graph. Model. 47 (2014) 8-17.

[16] L. Wang, E. Hua, M. Liang, C. Ma, Z. Liu, S. Sheng, M. Liu, G. Xie, W. Feng, Graphene sheets, polyaniline and AuNPs based DNA sensor for electrochemical determination of BCR/ABL fusion gene with functional hairpin probe, Biosens. Bioelectron. 51 (2014) 201-207.

[17] A.L. Liu, G.X. Zhong, J.Y. Chen, S.H. Weng, H.N. Huang, W. Chen, L.Q. Lin, Y. Lei, F.H. Fu, Z.L. Sun, X.H. Lin, J.H. Lin, S.Y. Yang, A sandwich-type DNA biosensor based on electrochemical co-reduction synthesis of graphene-three dimensional nanostructure gold nanocomposite films, Anal. Chim. Acta 767 (2013) 50-58.

[18] K.J. Feng, Y.H. Yang, Z.J. Wang, J.H. Jiang, G.L. Shen, R.Q. Yu, A nano-porous CeO< sub> 2</sub>/Chitosan composite film as the immobilization matrix for colorectal cancer DNA sequence-selective electrochemical biosensor, Talanta 70 (2006) 561-565.

[19] W. Zhang, T. Yang, X. Zhuang, Z. Guo, K. Jiao, Graphene sheets, polyaniline and AuNPs based DNA sensor for electrochemical determination of BCR/ABL fusion gene with functional hairpin probe, Biosens. Bioelectron. 24 (2009) 2417-2422.

[20] R. Pautler, E.Y. Kelly, P.J. Huang, J. Cao, B. Liu, J. Liu, Attaching DNA to nanoceria: regulating oxidase activity and fluorescence quenching, ACS Appl. Mater. Interfaces. 5 (2013) 6820-6825.

[21] Y. Hao, B. Zhou, F. Wang, J. Li, L. Deng, Y.N. Liu, Construction of highly ordered polyaniline nanowires and their applications in DNA sensing, Biosens. Bioelectron. 52 (2014) 422-426.

[22] S. Jampasa, W. Wonsawat, N. Rodthongkum, W. Siangproh, P. Yanatatsaneejit, T. Vilaivan, O. Chailapaku, Electrochemical detection of human papillomavirus DNA type 16 using a pyrrolidinyl peptide nucleic acid probe immobilized on screen-printed carbon electrodes, Biosens. Bioelectron. 54 (2014) 428-434.

[23] B. Rafique, A.M. Khalid, K. Akhtar, A. Jabbar, Interaction of anticancer drug methotrexate with DNA analyzed by electrochemical and spectroscopic methods, Biosens. Bioelectron. 44 (2013) 21-26.

[24] V.K. Gupta, P. Norouzi, H. Ganjali, F. Faridbod, M.R. Ganjali, Flow injection analysis of cholesterol using FFT admittance voltammetric biosensor based on MWCNT–ZnO nanoparticles, Electrochim. Acta 100 (2013) 29-34.

[25] P. Norouzi, V.K. Gupta, F. Faridbod, M. Pirali-Hamedani, B. Larijani, M.R. Ganjali, Carcinoembryonic Antigen Admittance Biosensor Based on Au and ZnO Nanoparticles Using FFT Admittance Voltammetry, Anal. Chem. 83 (2011) 1564-1570.

[26] P. Norouzi, B. Larijani, M. R. Ganjali, F. Faridbod, Admittometric electrochemical determination of atrazine by nano-composite immune-biosensor using FFT- square wave voltammetry. Int. J. Electrochem. Sci. 7 (2012), 10414-10426.

[27] M. Tichoniuk, D. Gwiazdowska, M. Ligaj, M. Filipiak, Electrochemical detection of foodborne pathogen Aeromonas hydrophila by DNA hybridization biosensor, Biosens. Bioelectron. 26 (2010) 1618-1623.

[28] D. Liu, Molecular detection of foodborne pathogens, CRC Press, 2009.

[29] S. Arora, R.K. Agarwal, B. Bist, Comparison of ELISA and PCR vis-à-vis cultural methods for detecting Aeromonas spp. in foods of animal origin, Int. J. Food. Microbiol. 106 (2006) 177-183.

[30] V. Singh, P. Somvanshi, G. Rathore, D. Kapoor, B.N. Mishra, Gene cloning, expression, and characterization of recombinant aerolysin from Aeromonas hydrophila, Appl. Biochem. Biotech. 160 (2010) 1985-1991.

[31] S. Tombelli, M. Mascini, C. Sacco, A.P.F. Turner, A DNA piezoelectric biosensor assay coupled with a polymerase chain reaction for bacterial toxicity determination in environmental samples, Anal. Chim. Acta 418 (2000) 1-9.

[32] M. Ligaj, M. Tichoniuk, D. Gwiazdowska, M. Filipiak, Electrochemical DNA biosensor for the detection of pathogenic bacteria Aeromonas hydrophila, Electrochim. Acta 128 (2014) 67-74.

[33] A.M. Fernandes, M.H. Abdalhai, J. Jia, B.W. Xi, J. Xie, J. Sun, R. Noeline, B.H. Lee, X. Sun, Development of highly sensitive electrochemical genosensor based on multiwalled carbon nanotubes-chitosan-bismuth and lead sulfide nanoparticles for the detection of pathogenic Aeromonas, Biosens. Bioelectron. 63 (2015) 399-406.

[34] X. Jing, Y. Wang, D. Wu, J. Qiang, Sonochemical synthesis of polyaniline nanofibers, Ultrason. Sonochem. 14 (2007) 75-80.

[35] S. Bhadra, D. Khastgir, N.K. Singha, J.H. Lee, Progress in preparation, processing and applications of polyaniline, Prog. Polym.Sci. 34 (2009) 783-810.

[36] A. S. Dezfuli, M. R. Ganjali, P. Norouzi, and F. Faridbod, Facile sonochemical synthesis and electrochemical investigation of ceria/graphene nanocomposites, J. Mater. Chem. B. 3 (2015) 2362–2370.

[37] G.M. Morris, R. Huey, W. Lindstrom, M.F. Sanner, R.K. Belew, D.S. Goodsell, A.J. Olson, AutoDock4 and AutoDockTools4: Automated docking with selective receptor flexibility, J. Comput. Chem. 30 (2009) 2785-2791.

[38] J. Sambrook, E. F. Fritsch, T. Maniatis, Molecular Cloning: A Laboratory Manual, Cold Spring Harbor Laboratory Press, Cold Spring Harbor, New York, 2nd edn., 1989.

[39] G. Wang, J. Bai, Y. Wang, Renzo, J. B. Bai, Preparation and electrochemical performance of cerium oxide-graphene nanocomposite as anode material for lithium ion battery, Scr. Mater. 65 (2011) 339-342.

[40] M. Srivastava, A.K. Das, P. Khanra, M.E. Uddin, N.H. Kim, J.H. Lee, Characterizations of in situ grown ceria nanoparticles on reduced graphene oxide as a catalyst for the electrooxidation of hydrazine, J. Mater. Chem. A 1 (2013) 9792-9801.

[41] P.H. Chen, R.L. McCreery, Control of Electron Transfer Kinetics at Glassy Carbon Electrodes by Specific Surface Modification, Anal. Chem. 68 (1996) 3958-3965.

[42] S.N. Topkaya, Gelatin methacrylate (GelMA) mediated electrochemical DNA biosensor for DNA hybridization, Biosens. Bioelectron. 64 (2015) 456-461.

[43] A.J. Bard, L.R. Faulkner, Electrochemical Methods. Fundamentals and Applications, Wiley, New York, 2nd edn, 2001.

[44] I.I. Suni, Impedance methods for electrochemical sensors using nanomaterials, Trends Anal. Chem. 27 (2008) 604-611.

[45] S. Zhang, Y. Ding, and H. Wei, Ruthenium polypyridine complexes combined with oligonucleotides for bioanalysis: a review, Molecules 19 (2014) 11933–11987.

[46] A. Erdem, k. Kerman, B. Meric, M. Ozsoz, Methylene blue as a novel electrochemical hybridization indicator, Electroanalysis 13 (2001) 219-223.

[47] A. Shi, J. Wang, X. Han, X. Fang, and Y. Zhang, A sensitive electrochemical DNA biosensor based on gold nanomaterial and graphene amplified signal, Sensors Actuators B Chem. 200 (2014) 206–212.

Figure legends

Fig. 1. XRD pattern of CeO_2NPs-RGO

Fig. 2. SEM image of CeO_2NPs before (a) and after combining with RGO (b)

Fig. 3. (A) CVs of 10mM $[Fe(CN)_6]^{3-/4-}$ containing 0.1M KCl at (a) bare GCE (b) CeO_2NPs-RGO/PANI/GCE (c) ssDNA /CeO_2NPs-RGO/PANI/GCE (d) ssDNA/CeO_2-RGO/PANI/GCE hybridized with 1×10^{-8} M targetDNA (**B)** Nyquist diagrams of 10 mM $[Fe(CN)_6]^{3-/4-}$ containing 0.1 M KCl at (a) bare GCE (b) CeO_2NPs-RGO/PANI/GCE (c) ssDNA/CeO_2NPs-RGO/PANI/GCE (d) ssDNA/CeO_2NPs-RGO/PANI/GCE hybridized with 1×10^{-8} M target DNA

Fig. 4. (A) The influence of ssDNA probe concentration in biosensor response (**B)** The influence of hybridization time in biosensor response. The error bars represent the standard deviation of five measurements RSD 4.5%.

Fig. 5. (A) FFT-SW peak current of 20 µM $[Ru(bpy)_3]^{2+/3+}$ recorded at (a) ssDNA/CeO_2NPs-RGO/PANI/GCE and after hybridization with different concentration of the target sequence (M) (b) 1×10^{-15} (c) 1×10^{-14} (d)1×10^{-13} (e)1×10^{-12} (f)1×10^{-11} (g)1×10^{-10} (h)1×10^{-9} (I)1×10^{-8} **(B)** Calibration curve, the plot of ΔI versus logarithm of target DNA concentration (M).

Fig. 6. FFT-SW peak current of 20 µM $[Ru(bpy)_3]^{2+/3+}$ recorded at (a) ssDNA/CeO_2NPs-RGO/PANI/GCE (b) ssDNA/CeO_2NPs-RGO/PANI/GCE hybridized with noncomplementary DNA (c) the electrode hybridized with two-base mismatch DNA sequence and (d) the electrode hybridized with target DNA (concentration of sequences: 1×10^{-8} M).

Fig. 7. Structure of single strand DNA and (a) 200 docking sites in 9 cluster ranks (b) most negative docking site, (c) electrostatic surface representation, part (d-f) are for double strands with similar discussion to single strand. Red and white color shows the negative and neutral charges.

Fig. 8. Expended docking sites and electrostatic surface for (a) and (c) single, (b) and (d) double strands.

Fig. 9. The response signal of biosensor of different concentration of extracted DNA from *A. hydrophila* (a) 10 µg mL^{-1} (b) 1 µg mL^{-1} (c) 0.1 µg mL^{-1} (d) 0.01 µg mL^{-1}. The error bars represent the standard deviation of five measurements for each concentration.

Table 1. Docking energies (kcal/mol) calculated by Autodock for interaction of $[Ru(bpy)_3]^{2+/3+}$ with single and double strands of 5′- GTGGTGGGCTGGGCGATCAA-3′.

Cluster rank	Lowest docking energy	Mean docking energy	Number of run in a cluster
Single			
1	-6.14	-6.11	149
2	-6.12	-6.09	32
3	-5.93	-5.93	2
4	-5.88	-5.88	1
5	-5.85	-5.85	1
6	-5.84	-5.81	12
7	-5.78	-5.78	1
8	-5.69	-5.69	1
9	-5.66	-5.66	1
Double			
1	-7.34	-7.31	58
2	-7.28	-7.23	3
3	-7.25	-7.21	40
4	-7.22	-7.2	6
5	-7.16	-7.15	4
6	-7.15	-7.12	7
7	-7.15	-7.12	22
8	-7.14	-7.14	1
9	-7.13	-7.13	2
10	-7.11	-7.09	10
11	-7.11	-7.1	3
12	-7.09	-7.07	13
13	-7.07	-7.07	1
14	-7.07	-7.06	19
15	-7.07	-7.06	9
16	-7.04	-7.04	1
17	-6.91	-6.91	1

Table 2. Comparison of different electrochemical DNA biosensors for detection of *A. hydrophila*

Electrode type	**Detection technique**	**Immobilization method**	**Detection limit**	**[Ref.]**
AuE	SWV	SAM	2.5 µg mL^{-1}	27
MWCNTs/CPE	SWV	Covalent bond	2 µg mL^{-1}	32
AuE		SAM	0.8 µg mL^{-1}	
MWCNT-Chi-Bi/GCE	DPV	Covalent bond	10 CFU(colony forming unit)	33
CeO_2-RGO/PANI/GCE	FFT-SWV	adsorption	0.01 µg mL^{-1}	This work

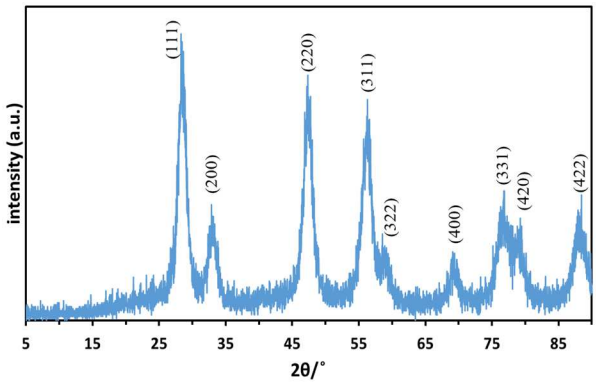

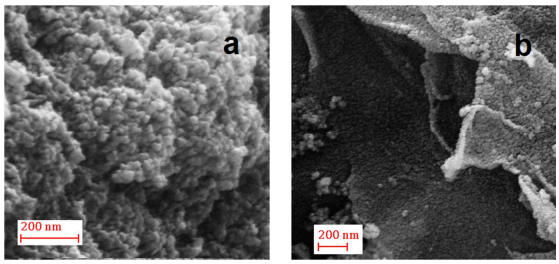

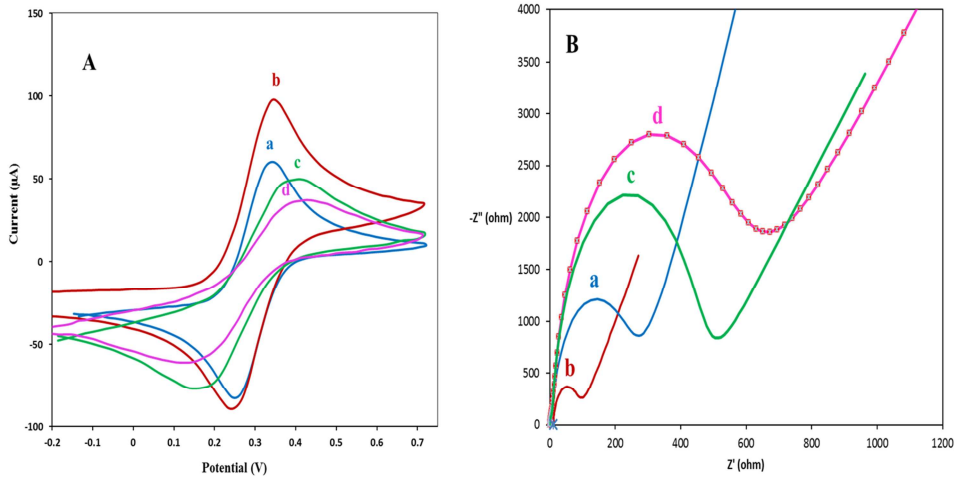

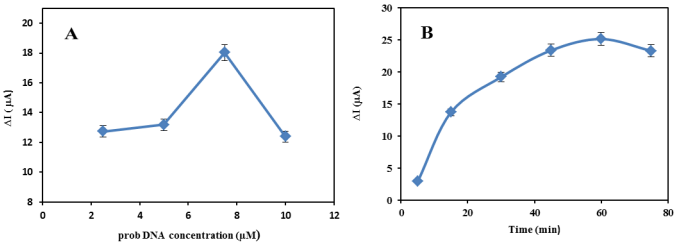

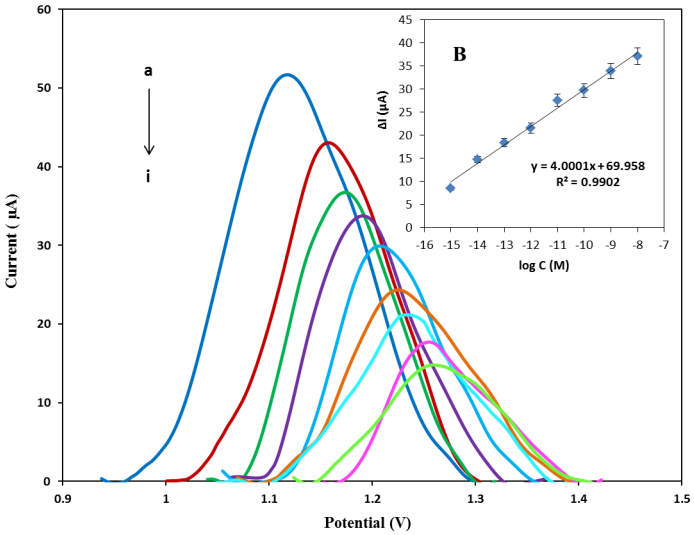

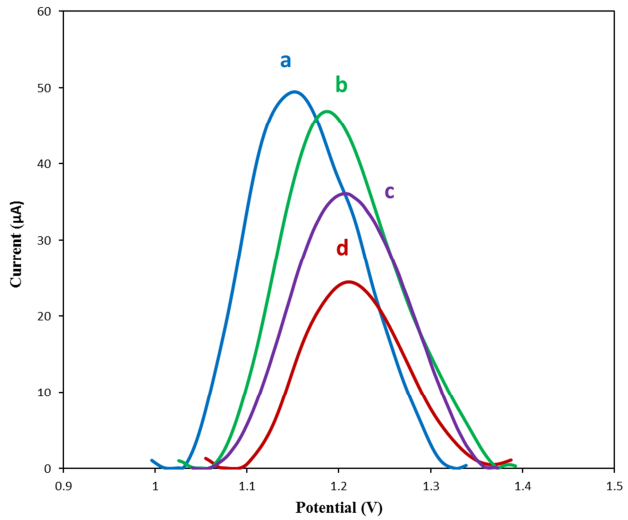

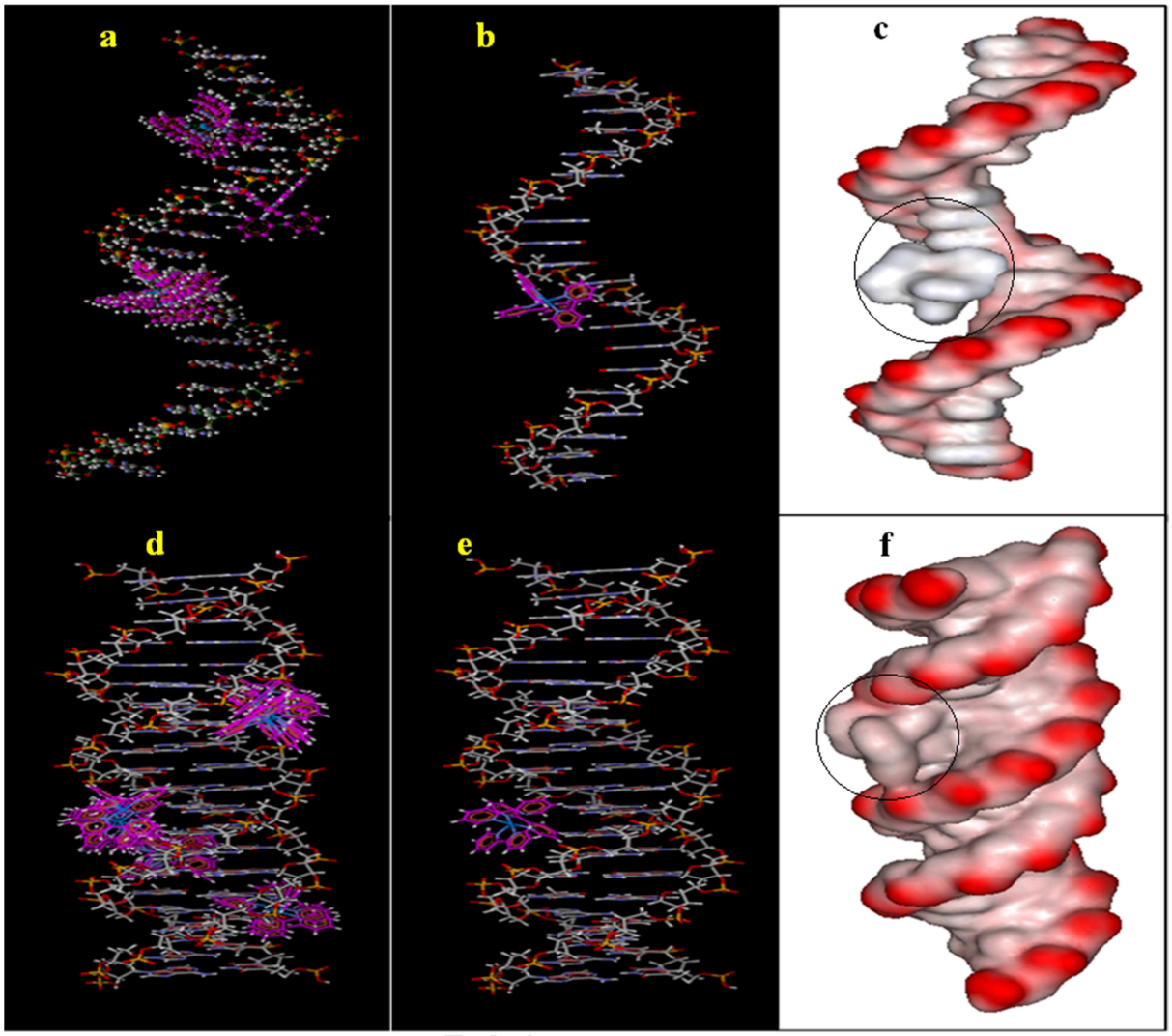

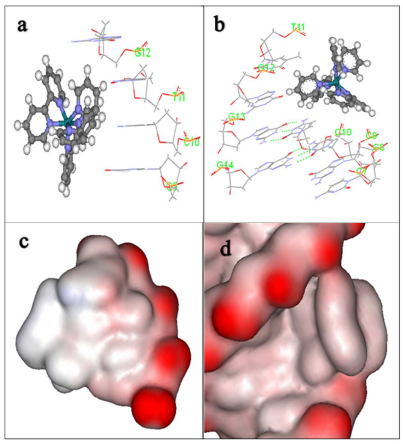

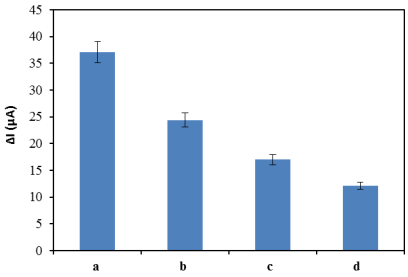

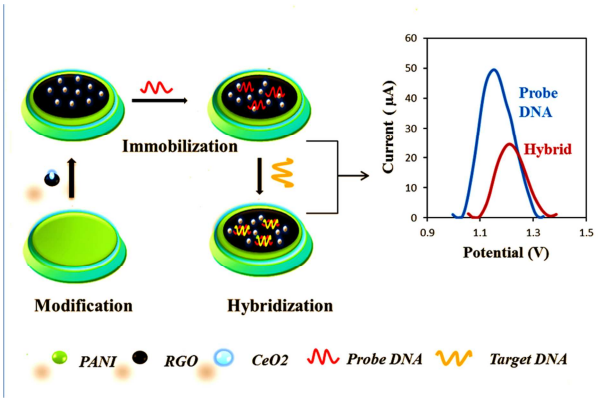

Research highlights

- New DNA biosensor is designed for sub-femtomolar detection of *Aeromonas hydrophila* DNA sequence.
- Reduced graphene oxide decorated Ceria nanoparticles was used as a new immobilization platform.
- Biosensor was successfully used to detect *Aeromonas hydrophila* DNA sequence in fish pond water.